Optimal Response of Isolated Multi-span Continous Deck Bridges Subjected to Near Fault and Far Field Events

Optimal response of isolated multi-span continous deck bridges subjected to near fault and far field events

Paolo Castaldo[1][0000-0002-7956-9392] and Elena Miceli[2][0000-0002-1262-3403]

[1] Politecnico di Torino, Turin, Italy
[2] Politecnico di Torino, Turin, Italy (corresponding author)
elena.miceli@polito.it

Abstract. The present study analyses the optimal friction coefficient for the seismic isolation of composite bridges, equipped with single concave friction pendulum (FPS) devices. The bridge is modelled through a six-degree-of-freedom system while the FPS friction property is described through a model that accounts for the dependency on the velocity. By introducing a time scale and a length scale, a nondimensional analysis has been used to solve the equations of motion. In detail, the response is analysed independently on the peak ground acceleration-to-velocity ratio. Furthermore, two different sets of seismic events are considered: far field and near fault. Then, many bridge models are analysed by changing different parameters (i.e., pier period, deck period, mass of the deck and of the pier and friction coefficient). By minimizing the substructure response, an optimum value of the friction coefficient is computed as function of the ratio between the period of the deck and the period of the seismic input.

Keywords: Multi-span continuous deck bridges, Seismic isolation, Non-dimensional equations, Seismic performance, Optimal friction coefficient, *PGA/PGV* ratio.

1 Introduction

One of the most effective strategies for enhancing the seismic performance of bridges involves the application of isolation techniques. The fundamental impact of this approach is the reduction of seismic inertia forces acting on the bridge deck and subsequently transmitted to the substructure. This is achieved by increasing the period of the isolation system [1],[2]. Friction pendulum system (FPS) bearings stand out due to their significant advantages: they decouple the isolation period from the deck mass and dissipate energy through friction between the concave surface and the slider [3]-[4].

Numerous studies have analysed the behaviour of FPS isolators, employing both experimental and numerical analyses [5]–[10]. For instance, in [11] different mathematical models are explored to represent bridge responses under real earthquake ground motions, demonstrating the accuracy of results when simplified approaches

are adopted to model the flexibility of piers and the deck. The work in [12] discusses the seismic performance improvement of a three-span continuous deck highway bridge using double concave friction pendulum devices. The study in [13] describes an experimental test on a 1:6 scale railway bridge isolated with friction pendulum bearings using a shake table. Three-dimensional models of multi-span steel girder bridges isolated with FPS devices are investigated in [14]. This study explores various modelling parameters, including geometrical and material characteristics of the bridge, and isolator design properties. Seismic reliability-based abacuses for the design of FPS devices in multi-span continuous deck bridges have been proposed in [15].

In the context of seismic isolation studies, Jangid [16]-[17] identified an optimal friction coefficient to design isolators in order to minimize structural responses during seismic events, considering both stochastic random processes and near-fault ground motions as seismic inputs. Subsequent research has delved into non-dimensional analyses of various structural systems based on key parameters. Non-dimensionalizations with respect to seismic input intensity for multi-span continuous deck bridges, isolated with single and double concave FPS devices, were proposed by [18] and [19], respectively. The frequency content of ground motions, represented by the *PGA/PGV* ratio, has been considered to assess optimal properties of FPS isolators for base-isolated buildings and bridges in, respectively, [20] and [21].

This study specifically examines the seismic performance of multi-span continuous composite deck bridges isolated with single concave FPS devices. The objective is to assess the influence of ground motion characteristics on the optimal friction coefficient of isolators through non-dimensionalization of motion equations with respect to the *PGA/PGV* ratio. A six-degree-of-freedom (dof) model is employed, encompassing 5 dofs for lumped masses of the RC pier and 1 additional dof for the composite deck, considered infinitely rigid. Two FPS devices are modeled on top of the elastic reinforced concrete (RC) pier and the rigid RC abutment, with the latter modeled as a fixed support. The velocity dependency of FPS device behavior is considered according to [5]. Record-to-record variability is incorporated by considering different sets of ground motions, including both far-field (FF) and near-fault (NF) inputs [20]. Moreover, a parametric analysis is conducted, covering the pier period, the ratio between the deck period and the period associated with the ground motion input, the friction coefficient, and the ratio between the mass of the deck and the pier. This analysis enables the assessment of normalized responses in terms of peak horizontal displacement of the pier and the calculation of the optimal value for the normalized friction coefficient of the isolators.

2 Equation of motions of the isolated bridge under seismic input

To simulate the response of multi-span continuous composite deck bridges isolated with single concave Friction Pendulum System (FPS) devices, a 6-degree-of-freedom (6-dof) system is employed (Fig. 1). Specifically, 5 degrees of freedom are allocated

for the elastic RC pier, and 1 degree of freedom is assigned to the rigid composite deck. The decision to represent the pier with five lumped masses is a compromise between computational efficiency and accuracy in evaluating the corresponding elastic response, as discussed in [18]. Two FPS devices are situated on top of the rigid and fixed RC abutment and on top of the pier.

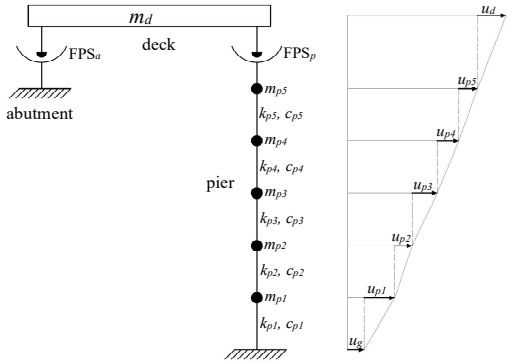

Fig. 1. Schematic representation of the 6 degree-of-freedom model of the isolated bridge.

The dimensional equations of motions along the longitudinal direction are:

$$m_d\ddot{u}_d(t)+m_d\ddot{u}_{p5}(t)+m_d\ddot{u}_{p4}(t)+m_d\ddot{u}_{p3}(t)+m_d\ddot{u}_{p2}(t)+m_d\ddot{u}_{p1}(t)+c_d\dot{u}_d(t)+F_p(t)+F_a(t)=-m_d\ddot{u}_g(t) \quad (1a)$$

$$m_{p5}\ddot{u}_{p5}(t)+m_{p5}\ddot{u}_{p4}(t)+m_{p5}\ddot{u}_{p3}(t)+m_{p5}\ddot{u}_{p2}(t)+m_{p5}\ddot{u}_{p1}(t)-c_d\dot{u}_d(t)+c_{p5}\dot{u}_{p5}(t)+k_{p5}u_{p5}(t)-F_p(t)=-m_{p5}\ddot{u}_g(t) \quad (1b)$$

$$m_{p4}\ddot{u}_{p4}(t)+m_{p4}\ddot{u}_{p3}(t)+m_{p4}\ddot{u}_{p2}(t)+m_{p4}\ddot{u}_{p1}(t)-c_{p5}\dot{u}_{p5}(t)-k_{p5}u_{p5}(t)+c_{p4}\dot{u}_{p4}(t)+k_{p4}u_{p4}(t)=-m_{p4}\ddot{u}_g(t) \quad (1c)$$

$$m_{p3}\ddot{u}_{p3}(t)+m_{p3}\ddot{u}_{p2}(t)+m_{p3}\ddot{u}_{p1}(t)-c_{p4}\dot{u}_{p4}(t)-k_{p4}u_{p4}(t)+c_{p3}\dot{u}_{p3}(t)+k_{p3}u_{p3}(t)=-m_{p3}\ddot{u}_g(t) \quad (1d)$$

$$m_{p2}\ddot{u}_{p2}(t)+m_{p2}\ddot{u}_{p1}(t)-c_{p3}\dot{u}_{p3}(t)-k_{p3}u_{p3}(t)+c_{p2}\dot{u}_{p2}(t)+k_{p2}u_{p2}(t)=-m_{p2}\ddot{u}_g(t) \quad (1e)$$

$$m_{p1}\ddot{u}_{p1}(t)-c_{p2}\dot{u}_{p2}(t)-k_{p2}u_{p2}(t)+c_{p1}\dot{u}_{p1}(t)+k_{p1}u_{p1}(t)=-m_{p1}\ddot{u}_g(t) \quad (1f)$$

where, $\ddot{u}_g(t)$ is the seismic input, u_i denote the displacement of the i-th lumped mass of the pier with respect to the subsequent inferior one, m_d signify the deck mass, m_i and k_i denote, respectively, the mass and stiffness of the i-th degree of freedom (dof) of the pier (assumed equal for all dofs), c_{pi} is the inherent viscous damping coefficient of each dof of the pier, c_d is the viscous coefficient of the bearing, t is the time instant, the dot indicates differentiation over time, and F_a and F_p are the resisting forces of the FPS devices placed on top of the abutment and the pier, respectively, expressed as [8]:

$$F_a(t)=\frac{m_d g}{2}\left[\frac{1}{R_a}\left(u_d(t)+\sum_{i=1}^{5}u_{pi}\right)+\mu_a\left(\dot{u}_d+\sum_{i=1}^{5}\dot{u}_{pi}\right)\mathrm{sgn}\left(\dot{u}_d+\sum_{i=1}^{5}\dot{u}_{pi}\right)\right] \quad (2a)$$

$$F_p(t)=\frac{m_d g}{2}\left[\frac{1}{R_p}u_d(t)+\mu_p(\dot{u}_d)\mathrm{sgn}(\dot{u}_d)\right] \quad (2b)$$

where μ denotes the sliding friction coefficient for the FPS bearing on the abutment (i.e., μ_a) or on the pier (i.e., μ_p) and can be modelled as function of the sliding velocity as follows, according to the experimental results in [4]-[5],[9]-[10],[22]:

$$\mu(\dot{u}) = f_{\max} - (f_{\max} - f_{\min}) \cdot \exp(-\alpha|\dot{u}|) \tag{3}$$

where f_{max} and f_{min} are the sliding coefficients at, respectively, large and zero velocity and it can be assumed f_{max} equal to $3f_{min}$, while α=30 is a parameter governing the transition from low to large velocities. In addition, the first part of both Eq.s (2a), (2b) represents the elastic component of the force, while the second addendum is the frictional component. In particular, the product mg is the gravity constant, R represents the radius of curvature of the FPS bearing on the abutment (i.e., R_a) or on the pier (i.e., R_p).

In this study, a non-dimensional analysis is proposed, drawing inspiration from the approaches outlined in [18]-[21]. Specifically, the dimensional terms of Eq.s (1a)–(1f) can be normalized using a time-scale equal to $1/\omega_g$ and a length-scale equal to a_0/ω_g^2, where ω_g is the representative circular frequency of the ground motion. In a simplified manner, ω_g is calculated as the ratio PGA/PGV and a_0 is representative of the seismic intensity and it stands for an acceleration.

By dividing Eq.s (1a)–(1f) for the mass of the deck and considering the previously defined time scale and length scale factors, the non dimensional equations can be obtained as follows:

$$\ddot{\psi}_d(\tau)+\ddot{\psi}_{p5}(\tau)+\ddot{\psi}_{p4}(\tau)+\ddot{\psi}_{p3}(\tau)+\ddot{\psi}_{p2}(\tau)+\ddot{\psi}_{p1}(\tau)+2\xi_d\frac{\omega_d}{\omega_g}\dot{\psi}_d(\tau)+\left[\frac{1}{2}\frac{\omega_d^2}{\omega_g^2}\psi_d(\tau)+\frac{\mu_p(\dot{u}_d)g}{2a_0}\operatorname{sgn}(\dot{\psi}_d)\right]+ \tag{4a}$$
$$+\left[\frac{1}{2}\frac{\omega_d^2}{\omega_g^2}\left(\psi_d(\tau)+\sum_{i=1}^{5}\psi_{pi}(\tau)\right)+\frac{g}{2a_0}\mu_a(\dot{u}_d+\sum_{i=1}^{5}\dot{u}_{pi})\left(\operatorname{sgn}\left(\dot{\psi}_d+\sum_{i=1}^{5}\dot{\psi}_{pi}\right)\right)\right]=-\ell(\tau)$$

$$\lambda_{p5}\left[\ddot{\psi}_{p5}(\tau)+\ddot{\psi}_{p4}(\tau)+\ddot{\psi}_{p3}(\tau)+\ddot{\psi}_{p2}(\tau)+\ddot{\psi}_{p1}(\tau)\right]-2\xi_d\frac{\omega_d}{\omega_g}\dot{\psi}_d(\tau)+2\xi_{p5}\frac{\omega_{p5}}{\omega_g}\lambda_{p5}\dot{\psi}_{p5}(\tau)+ \tag{4b}$$
$$+\lambda_{p5}\frac{\omega_{p5}^2}{\omega_g^2}\psi_{p5}(\tau)-\left[\frac{1}{2}\frac{\omega_d^2}{\omega_g^2}\psi_d(\tau)+\frac{\mu_p(\dot{\psi}_d)g}{2a_0}\operatorname{sgn}(\dot{\psi}_d)\right]=-\lambda_{p5}\ell(\tau)$$

$$\lambda_{p4}\left[\ddot{\psi}_{p4}(\tau)+\ddot{\psi}_{p3}(\tau)+\ddot{\psi}_{p2}(\tau)+\ddot{\psi}_{p1}(\tau)\right]-2\xi_{p5}\frac{\omega_{p5}}{\omega_g}\lambda_{p5}\dot{\psi}_{p5}(\tau)+2\xi_{p4}\frac{\omega_{p4}}{\omega_g}\lambda_{p4}\dot{\psi}_{p4}(\tau)+ \tag{4c}$$
$$-\lambda_{p5}\frac{\omega_{p5}^2}{\omega_g^2}\psi_{p5}(\tau)+\lambda_{p4}\frac{\omega_{p4}^2}{\omega_g^2}\psi_{p4}(\tau)=-\lambda_{p4}\ell(\tau)$$

$$\lambda_{p3}\left[\ddot{\psi}_{p3}(\tau)+\ddot{\psi}_{p2}(\tau)+\ddot{\psi}_{p1}(\tau)\right]-2\xi_{p4}\frac{\omega_{p4}}{\omega_g}\lambda_{p4}\dot{\psi}_{p4}(\tau)+2\xi_{p3}\frac{\omega_{p3}}{\omega_g}\lambda_{p3}\dot{\psi}_{p3}(\tau)-\lambda_{p4}\frac{\omega_{p4}^2}{\omega_g^2}\psi_{p4}(\tau)+\lambda_{p3}\frac{\omega_{p3}^2}{\omega_g^2}\psi_{p3}(\tau)=-\lambda_p \tag{4d}$$

$$\lambda_{p2}\left[\ddot{\psi}_{p2}(\tau)+\ddot{\psi}_{p1}(\tau)\right]-2\xi_{p3}\frac{\omega_{p3}}{\omega_g}\lambda_{p3}\dot{\psi}_{p3}(\tau)+2\xi_{p2}\frac{\omega_{p2}}{\omega_g}\lambda_{p2}\dot{\psi}_{p2}(\tau)-\lambda_{p3}\frac{\omega_{p3}^2}{\omega_g^2}\psi_{p3}(\tau)+\lambda_{p2}\frac{\omega_{p2}^2}{\omega_g^2}\psi_{p2}(\tau)=-\lambda_{p2}\ell(\tau) \tag{4e}$$

$$\lambda_{p1}\ddot{\psi}_{p1}(\tau)-2\xi_{p2}\frac{\omega_{p2}}{\omega_g}\lambda_{p2}\dot{\psi}_{p2}(\tau)+2\xi_{p1}\frac{\omega_{p1}}{\omega_g}\lambda_{p1}\dot{\psi}_{p1}(\tau)-\lambda_{p2}\frac{\omega_{p2}^2}{\omega_g^2}\psi_{p2}(\tau)+\lambda_{p1}\frac{\omega_{p1}^2}{\omega_g^2}\psi_{p1}(\tau)=-\lambda_{p1}\ell(\tau) \tag{4f}$$

Eq.s (4a)–(4f) are function of the following non dimensional parameters:

$$\Pi_{\omega_p}=\frac{\omega_p}{\omega_d},\ \Pi_{\omega_g}=\frac{\omega_d}{\omega_g},\ \Pi_{\lambda}=\lambda_p,\ \Pi_{\xi_d}=\xi_d,\ \Pi_{\xi_p}=\xi_{pi},\ \Pi_{\mu,a}=\frac{\mu_a\left(\dot{u}_d+\sum_{i=1}^{5}\dot{u}_{pi}\right)g}{a_0},\ \Pi_{\mu,p}=\frac{\mu_p(\dot{u}_d)\,g}{a_0} \qquad (5)$$

In the expressions of (5), the first term quantifies the level of isolation, while the second term signifies the ratio between the circular frequency of the isolated system and *PGA/PGV*. The terms ξ_i and ω_i have been previously elucidated. The last two terms, $\Pi_{\mu a}$ and $\Pi_{\mu p}$, represent the normalized friction coefficients. In this work, it is assumed that the two isolators have equal mechanical and geometrical properties. However, the corresponding normalized friction coefficients $\Pi_{\mu a}$ and $\Pi_{\mu p}$ are different since they refer to different sliding velocities. Thus, their peak values are used in their stead as follows: $\Pi_{\mu}^{*}=\Pi_{\mu,a}^{*}=\Pi_{\mu,p}^{*}=f_{\max}\,g/a_0$.

3 Parametric analysis

This section describes the different assumptions behind the parametric analysis both in terms of seismic inputs and bridge models.

According to the Performance-Based Earthquake Engineering (PBEE) approach [23]-[24], the performance of the structural system has to be predicted accounting for a wide range of possible ground motions. To this goal, the seismic input is herein given by the product of an intensity measure (IM) denoted as a_0 and a nondimensional function, such that the uncertainties of the seismic intensity are separated from those related to the characteristics of the record (i.e., record-to-record variability in addition to the event-to-event variability). In this study, the *PGA* has been selected as seismic intensity measure to achieve results useful in any site of the world where the seismic design is based on elastic pseudo-acceleration spectra according to the codes. For the purposes of this work, a group of 85 non-frequent natural ground motions has been selected, divided into two sets: the first set is made of 45 far-field (FF) records [25] and the second one is composed of 40 near-fault (NF) inputs [26]. In general, high *PGA/PGV* ratios are associated to seismic inputs of short durations and containing high energy content in the low period range while those with low *PGA/PGV* ratios are pulse-type motions with longer durations and contain high energy content in the high period range.

In addition, the seismic performance assessment involves the consideration of various ranges of structural parameters relevant to the problem. Specifically, the following parameter values are examined:

- 2 values of the pier period: T_p = 0.05s and 0.2s;
- 7 values of the period ratio: T_d/T_g = 2, 2.5, 3, 3.5, 4, 6, 8;
- 2 values of the mass ratio: λ_p = 0.1 and 0.2;
- 50 values of the normalized friction coefficient: Π_{μ}^{*} from 0 to 0.5.

Finally, in this work the normalized viscous damping factors inherent to the isolator and to the pier are set equal to, respectively, 0% and 5%.

Accounting for the different combinations of the parameters involved in the problem, a total number of 1400 different bridge models are considered. In addition, since 85 different seismic inputs have been included, a total number of 119000 numerical simulations in Matlab-Simulink [27] have been run.

4 Seismic response and optimal value of the friction coefficient

This section deals with the evaluation of the seismic response under different sets of excitations. In particular, the peak pier displacement in its normalized value is assumed as engineering demand parameter and computed as:

$$\psi_{p,\max} = \frac{u_{\mathrm{p,max}}\omega_g^2}{a_0} = \frac{\left|\left(\sum_{i=1}^{5} u_{pi}\right)\right|_{\max}\omega_g^2}{a_0} \tag{6}$$

In addition, it is demonstrated that this response parameter follows a lognormal distribution with mean value GM and dispersion β computed through the maximum likelihood technique [28]-[30] as follows:

$$GM\left(\Psi_{p,\max}\right) = \sqrt[N]{\delta_1 \cdot \ldots \cdot \delta_N} \tag{7}$$

$$\beta\left(\Psi_{p,\max}\right) = \sqrt{\frac{\left(\ln\delta_1 - \ln\left(GM\right)\right)^2 + \ldots + \left(\ln\delta_N - \ln\left(GM\right)\right)^2}{N-1}} \tag{8}$$

where δ represents the sample realization of the seismic response depending on the earthquake records, and, thus, $N=85$ is the total number of seismic inputs. Finally, the k-th percentile of the response parameter is calculated as:

$$\delta_k = GM\left(\Psi_{p,\max}\right)\cdot\exp\left[t\left(k\right)\cdot\beta\left(\Psi_{p,\max}\right)\right] \tag{9}$$

where $t(k)$ is equal to 0,1 and -1 for k equal to the 50th, 16th and 84th percentile.

In Fig. 2, Fig. 3, Fig. 4 the geometric mean of the normalized peak pier displacement is shown as function of the maximum normalized friction coefficient and for fixed values of the other involved parameters, considering, respectively, far field, near fault and all the 85 seismic inputs together. As a general observation, $GM(\Psi_{p,max})$ is larger when the ratio T_d/T_g decreases, especially, for low values of the maximum normalised friction coefficient. The reason for this behaviour is that the lower is the period of the deck with respect to the ground motion period, the larger are the forces acting on the deck and thus transmitted to the substructure. In addition, the geometric mean of the normalized peak displacement of the pier increases for larger values of T_p whereas decreases for larger values of λ_p, since this growth determines a decrease in

the forces transmitted from the deck to the pier. However, the influence of the mass ratio is remarkable, especially, for low pier periods.

All these considerations are valid for all the different sets of seismic records, confirming the assumption that the record selection does not influence the response if the proper time and length scales are adopted. The differences are in terms of order of magnitude, since large *PGA/PGV* ratios imply larger pier responses.

In addition, in all the figures there is a decrease followed by an increase in the response for increasing values of the normalized friction coefficient. In correspondence of this minimum value it is possible to recognize an optimal value for the friction coefficient able at minimizing the substructure response, as also analyzed in [18]-[21].

The existence of this optimum value derives from the equilibrium between two counteracting effects: on the one hand, there is an increase of the substructure response because higher modes participate and also due to the increase of the isolator strength, determining larger forces transmitted to the pier due to the higher equivalent stiffness of the isolation system; on the other hand, the larger the friction coefficient the larger the dissipation capacity of the isolator and, thus, the lower the substructure response. It is important to underline that the orders of magnitude of the response parameter are different, but the optimum value of the normalized friction coefficient is substantially found in the same range for all the sets of the records considered, and for different values of the mass ratio and pier period. On the other hand, the optimal value of the normalized friction coefficient, herein indicated as $\Pi^*_{\mu,opt}$, is assumed to be influenced by the period ratio (i.e., T_d/T_g).

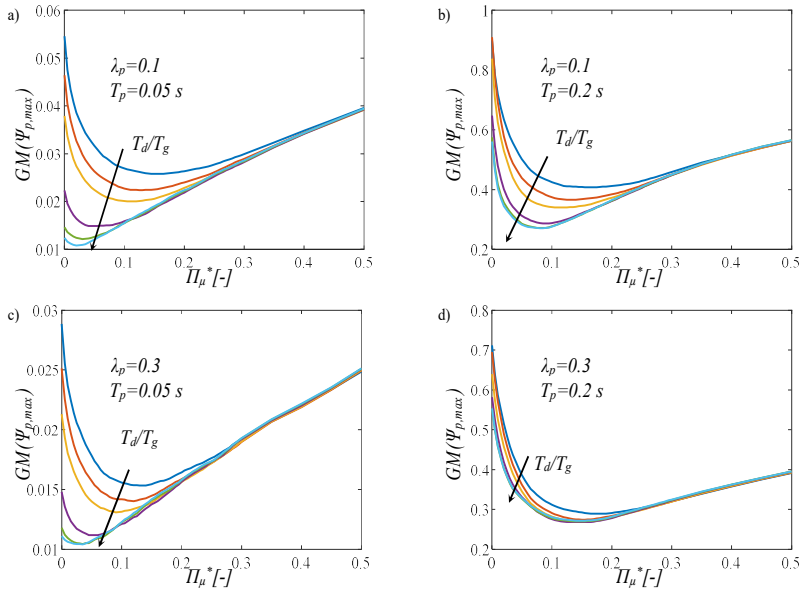

Fig. 2. Geometric mean of the of the pier seismic response in terms of maximum normalized friction coefficient considering FF seismic records and fixed values of the other parameters.

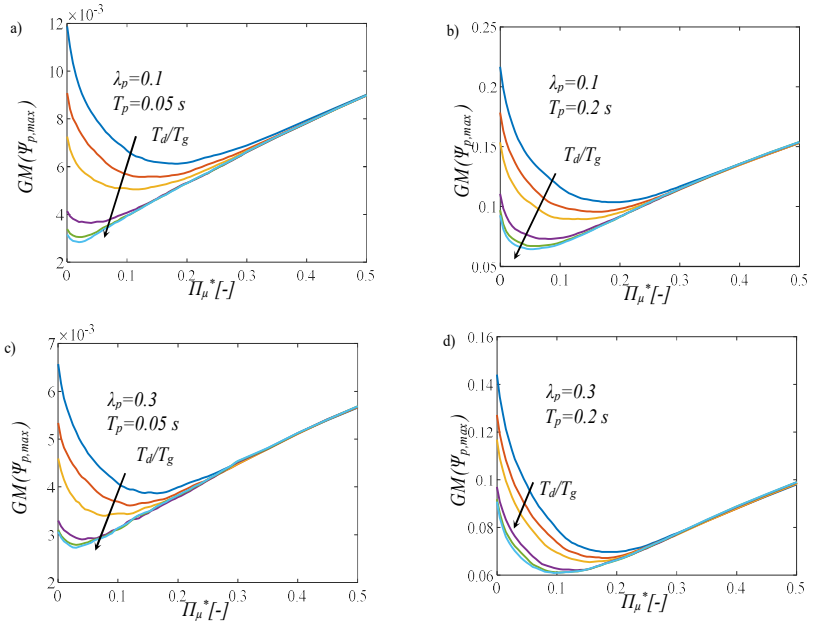

Fig. 3. Geometric mean of the of the pier seismic response in terms of maximum normalized considering NF seismic records and fixed values of the other parameters.

Starting from the previous considerations, in Fig. 5 a regression of the data is performed in order to evaluate the optimum value of the friction coefficient able at minimizing the 16th, 50th, and 84th percentile as function of the only influencing parameter (i.e., T_d/T_g). In detail, it is possible to observe that the optimum value decreases with larger T_d/T_g ratios, since the normalized response of the substructure is lower as a consequence of the isolation effectiveness.

Future works should extend the parametric analysis including more values of the period ratio T_d/T_g, of the mass ratio λ_p and of the pier period T_p.

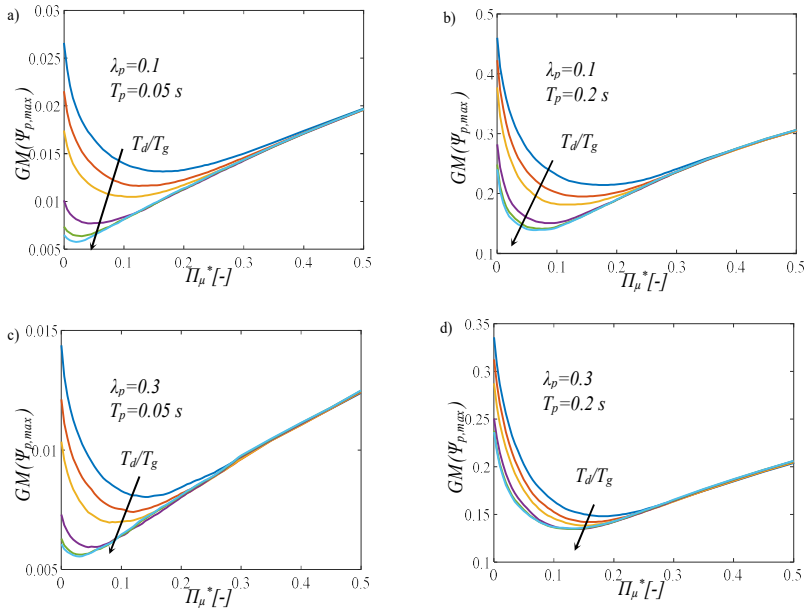

Fig. 4. Geometric mean of the of the pier seismic response in terms of maximum normalized considering FF+NF seismic records and fixed values of the other parameters.

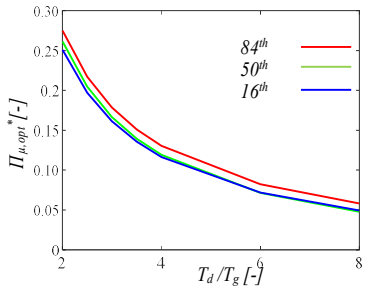

Fig. 5. Regression of the optimum normalized friction coefficient considering all the percentiles and including both far field and near fault records.

5 Conclusions

This study aims to assess the optimal properties of single concave friction pendulum (FPS) bearings used for seismic isolation in multi-span continuous composite deck bridges. Ground motion characteristics are considered through the peak ground acceleration (*PGA*) and the parameter T_g, expressed as a function of the peak ground acceleration-to-velocity (*PGA/PGV*) ratio. These parameters serve as length scale and time

scale factors, forming the basis for a non-dimensional formulation to evaluate the normalized response of a six-degree-of-freedom structural model under various seismic events. Two families of ground motions corresponding to near-fault and far-field seismic records are analyzed. A diverse set of natural records is chosen to account for record-to-record and event-to-event variability. Several bridge systems are examined by varying the pier fundamental period, the ratio between the fundamental period of the isolated deck and the period of the ground motion, the mass ratio, and the normalized friction coefficient. The normalized response of the pier is strongly influenced by the period ratio, with an inverse proportionality. In addition, the response trends for the substructure are remarkably similar across different sets of records. Far-field records are more demanding due to their pulse-type nature covering a wider frequency range. Furthermore, optimal values of the normalized friction coefficient are determined to minimize different percentiles of the normalized pier displacement. These optimal values decrease with larger period ratio values and are not significantly affected by other bridge parameters. Moreover, optimal coefficients remain consistent across different record sets, highlighting the effectiveness of the *PGA/PGV* ratio.

References

1. Ghobarah A, Ali HM (1988) Seismic performance of highway bridges. Engineering Structures 10.
2. Tsopelas P, Constantinou MC, Okamoto S, Fujii S, Ozaki D (1996) Experimental study of bridge seismic sliding isolation systems. Engineering Structures 18 (4):301-310.
3. Tongaonkar NP, Jangid RS (2003) Seismic response of isolated bridges with soil–structure interaction. Soil Dynamics and Earthquake Engineering 23:287-302.
4. Zayas VA, Low SS, Mahin SA (1990) A simple pendulum technique for achieving seismic isolation. Earthquake Spectra1990 6(2):317–33.
5. Mokha A, Constantinou MC, Reinhorn AM (1990) Teflon Bearings in Base Isolation. I: Testing. Journal of Structural Engineering 116(2):438-454.
6. Constantinou MC, Mokha A, Reinhorn AM (1990) Teflon Bearings in Base Isolation. II: Modeling. Journal of Structural Engineering 116(2):455-474.
7. Almazàn JL, De la Llera JC (2003) Physical model for dynamic analysis of structures with FPS isolators. Earthquake Engineering and Structural Dynamics 32(8):1157–1184.
8. Mosqueda G, Whittaker AS, Fenves GL (2004) Characterization and modeling of Friction Pendulum bearings subjected to multiple components of excitation. Journal of Structural Engineering 130(3):433-442.
9. Jangid RS (2005) Computational numerical models for seismic response of structures isolated by sliding systems. Structural Control and Health Monitoring 12:117–137.
10. Jangid RS (2008) Stochastic response of bridges seismically isolated by friction pendulum system. Journal of Bridge Engineering 13(4):319.
11. Kunde MC, Jangid RS (2006) Effects of pier and deck flexibility on the seismic response of isolated bridges. Journal of Bridge Engineering 11(1):109-121.
12. Kim YS, Yun CB (2007) Seismic response characteristics of bridges using double concave friction pendulum bearings with tri-linear behaviour. Engineering Structures 29:3082-3093.

13. Meng D, Yang M, Yang Z, Chouw N (2022) Effect of Earthquake-induced Transverse Poundings on a 32 m Span Railway Bridge Isolated by Friction Pendulum Bearings. Engineering Structures 251:113538.
14. Eröz M, DesRoches R (2013) The influence of design parameters on the response of bridges seismically isolated with the friction pendulum system (FPS). Engineering structures 56:585-599.
15. Castaldo P, Amendola G, Giordano L, Miceli E (2022) Seismic reliability assessment of isolated multi-span continuous deck bridges. Ingegneria Sismica - International Journal of Earthquake Engineering 3.
16. Jangid RS (2000) Optimum frictional elements in sliding isolation systems. Computers and Structures 76(5):651–661.
17. Jangid RS (2005) Optimum friction pendulum system for near-fault motions. Engineering Structures 27(3):349–359.
18. Castaldo P, Amendola G (2021) Optimal Sliding Friction Coefficients for Isolated Viaducts and Bridges: A Comparison Study. Structural Control and Health Monitoring 28(12).
19. Castaldo P, Amendola G (2021) Optimal DCFP bearing properties and seismic performance assessment in nondimensional form for isolated bridges. Earthquake Engineering and Structural Dynamics 50(9):2442-2461.
20. Castaldo P, Tubaldi E (2018) Influence of Ground Motion Characteristics on the Optimal Single Concave Sliding Bearing Properties for Base-isolated Structures. Soil Dynamics and Earthquake Engineering 104:346-64.
21. Castaldo P, Miceli E (2023) Optimal Single Concave Sliding Device Properties for Isolated Multi-Span Continuous Deck Bridges Depending on the Ground Motion Characteristics. Soil Dynamics and Earthquake Engineering 173:108128.
22. Constantinou MC, Whittaker AS, Kalpakidis Y, Fenz DM, Warn GP (2007) Performance of Seismic Isolation Hardware Under Service and Seismic Loading. Technical Report MCEER-07-0012.
23. Aslani H, Miranda E (2005), Probability-based seismic response analysis. Engineering Structures 27(8):1151-1163.
24. Porter KA (2003) An overview of PEER's performance-based earthquake engineering methodology. Proceedings of the 9th International Conference on Application of Statistics and Probability in Civil Engineering (ICASP9), San Francisco, California.
25. Tso WK, Zhu TJ, Heidebrecht AC (1992) Engineering implication of ground motion A/V ratio. Soil Dynamics and Earthquake Engineering 11(3):133-144.
26. PEER Ground Motion Database Web Application Beta Version – October 1, 2010.
27. Math Works Inc. (1997) MATLAB-High Performance Numeric Computation and Visualization Software. User's Guide. Natick: MA, USA.
28. Troisi R, De Simone S, Vargas M, Franco M (2022) The other side of the crisis: organizational flexibility in balancing Covid-19 and non-Covid-19 health-care services. BMC Health Services Research 22(1):1096.
29. Troisi R, Alfano G (2023) Is "justice hurried actually justice buried"? An organisational perspective of the Italian criminal justice. International Journal of Public Sector Management 36(1): 94–109.
30. Troisi R, De Simone S, Franco M (2023) Illegal firm behaviour and environmental hazard: The case of waste disposal, European Management Review, 10.1111/emre.12600.